Formation of Hydroxyapatite via Transformation of Amorphous Calcium Phosphate in The Presence of Alginate Additives

*Seniz Ucar**, [a] Sindre H. Bjørnøy,[b] David C. Bassett,[b,c] Berit L. Strand,[d] Pawel Sikorski,[b] and Jens-Petter Andreassen** [a].*

[a] Department of Chemical Engineering, [b] Department of Physics and [d] Department of Biotechnology, Norwegian University of Science and Technology, Trondheim, Norway. [c] Department of Chemical Engineering, University of Birmingham, Birmingham, UK.

KEYWORDS. Amorphous calcium phosphate, hydroxyapatite, biomineralization, alginate

ABSTRACT

Hydroxyapatite (HA) is the primary mineral of vertebral tooth and bone tissue, thus, it is often incorporated into synthetic composite materials designed for hard tissue engineering applications. Understanding the formation mechanisms of apatitic minerals and the effects of matrix molecules during mineralization is vitally important to instruct the design of synthetic biomaterials. Here we explore the mechanism of HA formation via an amorphous calcium phosphate (ACP) precursor and the effects of alginate-based additives on the reaction progression. We found that in additive-

free experiments the solution speciation was dominated by the classical formation of ion pairs prior to the emergence of an ACP phase, which was then followed by a transformation to HA. In the presence of alginate-based additives, ACP formation was retarded by several orders of magnitude due to kinetic hinderance and possible stabilization of intermediates, depending on the functionality of the molecules. ACP lifetime was also prolonged in the presence of additives and this stabilizing effect was associated with the surface adsorption capacity of the additives which suggests a solvent-mediated transformation mechanism. When additives with G-units were introduced in the system, the final precipitates were composed of a mixture of octacalcium phosphate (OCP) and HA via effective suppression of HA formation. Our results demonstrate that compositional variations in the additive molecules strongly influence mineralization pathways.

INTRODUCTION

Calcium phosphates (CaP) are an important class of biological minerals found in natural hard tissues; among them hydroxyapatite (HA) is the dominant mineral phase in mammalian calcified tissues. Consequently, composite biomaterials designed for bone tissue engineering applications often incorporate either HA or a precursor CaP phase that can transform to HA under *in vivo* conditions. Understanding the formation mechanisms of apatitic minerals and the effects of organic components on the crystallization process can inform the development of improved biomaterials,[1] *in vitro* model systems of biomineralization,[2] and may also inspire new routes for the syntheses of non-biogenic minerals.[3, 4]

Extensive studies on the nucleation mechanisms of biological HA agree that rather than forming directly from solution, HA follows a crystallization pathway via an amorphous calcium phosphate (ACP) precursor.[5, 6] However, there is an ongoing debate regarding how this ACP-mediated process is driven, from the initial formation of ACP to its transformation to HA.

Posner's clusters, $Ca_9(PO_4)_6$, were initially proposed as the building blocks for ACP, and samples from both synthetic and biological systems have been shown to contain these ion clusters.[6] However, further studies also proposed that other prenucleation species and ACP phases that vary in structure and chemical composition depending on the reaction conditions, may be present.[7, 8] Several hypotheses regarding the mechanism of ACP formation have been suggested. According to classical theory, amorphous phases form under conditions of high supersaturation where the critical nucleus size falls below the crystal unit size.[9] Alternative pathways proposed in the literature include: 1) stable prenucleation clusters which aggregate to form ACP [10], 2) the presence of soluble ion-complexes that lead to ACP precipitation by aggregating and consuming extra calcium ions from solution [11], and 3) a two-step mechanism that includes the formation of an initial ACP phase via ion-complexes that later transforms into a second ACP phase through densification.[12]

The presence of additives in the reaction medium can affect ACP formation via different mechanisms in correlation with the proposed formation pathway. Additives can interfere with the kinetic variables of classical nucleation (i.e. collision frequency) that results in prolonged induction times, or can promote ACP nucleation by acting as favorable substrates for nucleation.[13] Alternatively, for ACP formation pathways via aggregation and maturation of ion association clusters, additives can suppress the reaction progression by influencing aggregation, dehydration and/or complexation mechanisms through electrostatic interactions.[10, 11] When polymeric additives

are present in the reaction medium, they can evoke metastable, dense liquid-like precursors known as polymer induced liquid precursors (PILP).[14, 15] According to this process, polymeric entities can sequester ions to induce the formation of an amorphous precursor phase that would otherwise be unstable in the system.[16] The amorphous phase formed via the PILP mechanism features a fluidic character that has been attributed to a highly hydrated nature.[14] However, a recent study by Xu *et al.* has proposed PILP to be a polymer-driven assembly of ~2 nm solid clusters and attributed its liquid-like behavior to the small size and surface properties of the assemblies.[17] PILP is considered to be an important mechanism in biologically controlled mineralization (especially for bone formation) and previous studies have shown its particular significance for synthetic CaP biomineralization systems.[15, 18]

The transformation mechanism of the ACP precursor to HA is also a subject of active debate and multiple mechanisms have been proposed. According to classical crystallization theory, phase transformation is governed by the chemical potential difference between phases (i.e. activity based supersaturation), and can either follow a dissolution-reprecipitation pathway in solution or a solid state transformation; the latter being particularly common at high temperatures.[19, 20] Solvent mediated phase transformation through dissolution- reprecipitation reactions can be governed either by dissolution of the metastable phase or nucleation and growth of the stable phase depending on supersaturation and the relative kinetics of the individual reactions, as modeled by Cardew and Davey.[21] In an attempt to describe phenomena occurring during transformation, various alternative or 'nonclassical' mechanisms have also been suggested. For example, Tang *et al.* proposed a solution mediated surface nucleation process whereby HA heterogeneously nucleates on ACP, but the transformation rate in these studies was stated to be a function of the amount of initial ACP formed and calcium activity in solution, rather than solution

supersaturation.[22-25] Xie *et al.* and Wang *et al.* proposed an alternative mechanism whereby HA nucleation takes place within the ACP precursor through a solid-solid transformation.[12, 26] In these theories the kinetics of transformation are also not directly linked to the solution supersaturation.

The various proposed mechanisms to describe ACP-mediated HA formation infer different roles of additives in this process. The presence of additives can stabilize or destabilize ACP by effecting its dissolution rate, effect the nucleation rate of HA, or influence the chemistry and solubility of the ACP phase, which consequently influences the solution supersaturation from a classical point of view.[19, 27] In contrast, if the phase transformation is independent of supersaturation, as proposed by some studies, or involves rearrangement of building units of the solid, additives are thought to stabilize the ACP phase through surface interactions.[28] This may occur either by interfering with the surface nucleation of HA or limiting the mass transfer between the solid and solution.[12, 24]

Recent studies in our group have focused on the development of composite biomaterials comprised of alginate hydrogels with CaP minerals.[29] Alginate is a polysaccharide polymer which is composed of 1-4 linked β-D-mannuronic acid (M) and α-L-guluronic acid (G) residues with an alternating or block structure. The M- and G- units of alginate differ in the configuration of carboxyl groups that in turn highly affects their functionality. Calcium ions show specific affinity towards the outward carboxyl groups of the G- units of alginate, and bind to G-blocks and alternating blocks of the polymer but not to M-blocks.[30] Therefore, the way in which alginate regulates mineralization is highly dependent on its chemical composition, sequential structure of the repeating units and molecular weight. Spatiotemporal analysis of the evolution of CaP phases within the hydrogel network at room temperature demonstrated precipitation of ACP as a metastable precursor and its transformation to more stable crystalline phases such as brushite, octacalcium phosphate (OCP) and HA depending on the reaction conditions.[31] In addition, our

detailed kinetic investigations on the transformation of brushite to HA generated new questions regarding the formation pathway of HA, such as the nucleation mechanism and the roles of ACP precursor and alginate additives in nucleation.[32] Thus, the present study aims to explore the mechanism underlying HA formation via an amorphous precursor in the presence of alginate additives. For this purpose, the effects of alginate additives with varying molecular weight and functionality have been investigated to shed light on the operating mechanism(s) of the chosen matrix molecule on HA formation.

EXPERIMENTAL

Materials

All chemical reagents were purchased from Sigma-Aldrich (Sigma-Aldrich Norway AS, Oslo, Norway) unless stated otherwise. Ultrapure deionized water (DIW) was used to prepare all aqueous solutions. Alginate, isolated from *Laminaria hyperborea (L.hyp)* stipe, was obtained from FMC Biopolymer (Norway) with a molecular mass of 274 kDa and 68% G content. Two different oligomers of alginate, denoted as G- and M-blocks, consisted of 90% and 5% G monomer, respectively, with the degree of polymerization ≈ 20 for both and a molecular mass of ≈ 3500 Da. The G-blocks were produced from *L. hyp* stipe alginate by acid degradation and fractionation as decribed previously.[33] The M-blocks were produced from alginate from *Ascophyllum nodosum* by acid degradation and calcium fractioning as described previously.[34]

Methods

All experiments were carried out in a magnetically stirred 0.5 L double-walled glass reactor, and two baffles were attached to the lid. Temperature was controlled by a water bath at 25°C for all experiments. Nitrogen, saturated with water, was constantly bubbled into solutions 2 h prior to and during the experiments to exclude atmospheric carbon dioxide. The chemical speciation and activity based supersaturation (*S*) were determined by the thermodynamic calculation programs PHREEQC Interactive 3.1 (U.S. Geological Survey, Reston, VA, USA) and Minteq 3.0 (KTH, Royal Institute of Technology, Stockholm, Sweden), using the Minteq v4 database (Equation 1). The equilibrium constants used for solution speciation are given in the supplementary information (section A).

$$S = \left(\frac{IAP}{K_{sp}}\right)^{\frac{1}{\upsilon}} \qquad \text{(Eq. 1)}$$

IAP represents the ionic activity product in solution, K_{sp} is the solubility product and υ is the number of ions in one mole of the corresponding compound.

The pH was recorded continuously by means of a combined glass electrode with a KCl reference electrolyte and calcium ion activity in the vessel was monitored online via a calcium ion specific electrode with Tiamo^{TM} software (Metrohm AG, Herisau, Switzerland) (see supplementary information section B).

Dynamic light scattering (DLS) and zeta potential measurements were performed using a Zetasizer Nano ZS (Malvern Panalytical Ltd., Malvern, UK) by simultaneous sampling from the reaction solution (see supplementary information section C). Transmission electron microscopy (TEM) was performed using a JEOL JEM 2100 microscope fitted with a LaB_6 cathode (JEOL, Tokyo,

Japan) at an accelerating voltage of 200 kV. Samples were prepared by drop-casting onto carbon coated copper TEM grids at various time points during the reactions. Diffraction patterns were analyzed using DiffTools in Digital Micrograph software (version 2.32, Gatan).

Characterization of solid phases were conducted via powder X-ray Diffraction (XRD) (D8 Advance, Bruker AXS GmBH, Karlsruhe, Germany) in the 2θ range of 4-75°with a step size of 0.013° and a step time of 0.67 s. Fourier transform infrared (FTIR) (Tensor, Bruker AXS GmBH, Karlsruhe, Germany) spectra of powder samples were collected between 4000-550 cm^{-1}. Raman microspectroscopy (InVia Reflex, Renishaw, Gloucestershire, England) was performed (2 s integration time, 50 accumulations) using a 535 nm laser through a 10x lens.

Spontaneous precipitation of calcium phosphate was achieved in batch experiments by preparing supersaturated solutions (S_{HA}= 25.6) and allowing precipitation to occur under constant stirring (300 rpm). The initial supersaturation of the working solution was determined by scanning through a range of values between S_{HA}= 17.1- 34.0 in accordance with the previous studies of HA formation in our group, and choosing the supersaturation at which the two-step precipitation behavior was observed following an induction period of approximately 15 min and the reaction was completed within 4 h, for experimental practicality. For this, a phosphate solution (2.4 mM KH_2PO_4) containing KNO_3 (50 mM) for ionic strength adjustment and KOH to adjust the final solution pH to 7.40 ± 0.02, was prepared from its stock to a total volume of 250 mL. In experiments with alginate additives, the corresponding amount of filtered polymer solution (1 mg L^{-1}) was also added to the phosphate solution initially. A calcium solution (20 mL, 50 mM $Ca(NO_3)_2.4H_2O$) was then added in the reaction medium at a rate of 150 mL min^{-1} via an automated dosing unit (907 Titrando, Metrohm AG, Herisau, Switzerland). Titration experiments were conducted with lowering the calcium addition rate to 0.4 mL min^{-1} under the same experimental conditions. All

experiments were conducted in replicates (see supplementary information Figure S1) and solutions were freshly prepared for each experiment with Milli-Q water (resistivity 18.2 MΩ cm at 25°C). The viscosity measurements of additive free Milli-Q water and 1 ppm solutions of alginate-based additives were performed using a rheometer (Physica MCR 100, Anton Paar, Graz, Austria).

RESULTS &DISCUSSION

Progression of the reaction

Calcium phosphate crystallization was investigated by allowing spontaneous precipitation from supersaturated solutions while simultaneously monitoring the pH and calcium activity profiles. Successive steps of the reaction were identified via the distinct drops in either of the monitored signals, which indicated the occurrence of separate phases with characteristic calcium solubility (Figure 1). Supersaturated solutions were prepared by the instantaneous addition of a calcium solution (20 mL, 150 mL min^{-1}) to a stirred phosphate solution at time 0 and after equilibration, both pH and calcium activity remained stable during stage 1 (s1). The first discernable drop in either signal was interpreted as evidence of the first nucleation event, which indicated the appearance of the first new phase from the solution. This point determined the onset of stage 2 (s2). The second abrupt drop in the monitored signals was accordingly interpreted as a second nucleation event and the emergence of a second separate phase in the system. This point determined the onset of stage 3 (s3). Any units (clusters) formed in the solution before the first nucleation point, i.e. during s1, are termed prenucleation species in this context. Detailed analyses were conducted to identify the chemical and structural progression of precipitates that correspond to the distinct stages of the reaction.

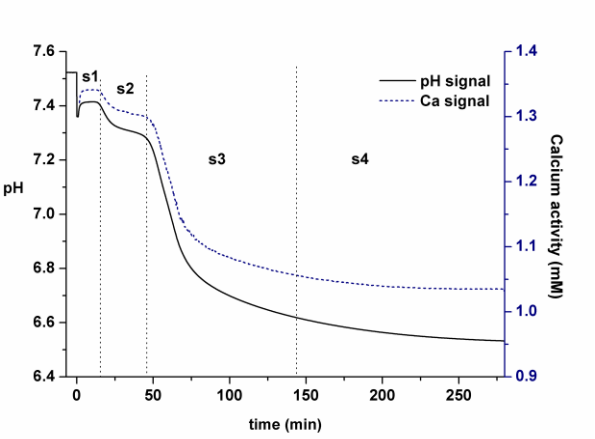

Figure 1. The pH and calcium activity monitored as a function of time during the spontaneous precipitation reaction. Curves were sectioned in four stages (labeled s1-s4) in accordance with distinct changes recorded in signal profiles.

Addition of calcium ions to the reaction medium resulted in an immediate drop in pH, followed by a short rebound and gradual leveling off in the beginning of s1. Since the pH of the system is a function of phosphate speciation, changes in pH were interpreted in terms of changing ratios of the phosphate species.[26] Upon addition of calcium in the reaction medium, ion pairs form between calcium ions and phosphate species. Thermodynamic calculations showed that under the specified experimental conditions, dominant ion pair was $[CaHPO_4]^0$, and concentrations of $[CaH_2PO_4]^+$ and $[CaPO_4]^-$ were negligible. The concentration based ratio of $[H_2PO_4^-]/ [HPO_4^{2-}]$ in solution was 0.26 before calcium addition, and the ratio of ion pairs $[CaH_2PO_4]^+ / [CaHPO_4]^0$ that formed with the addition of calcium was 0.038. As the calculations demonstrated, the overall decrease in pH can be explained by the formation of ion pairs that changed the ratio of free phosphate species towards a lower $[HPO_4^{2-}]$ content (see supplementary information Figure S2). The fluctuations in pH before its stabilization has previously been attributed to the possible formation of unstable clusters and solids due to local areas of high supersaturation created by the addition of calcium

solution, which then immediately dissociate to establish an equilibrium.[26, 35] The drop of pH below the equilibrium value followed by its fast rebound supported a similar mechanism indicating formation of highly unstable solution species and/or solid upon fast addition of calcium (Figure 2A). Due to the slow dehydration rate of calcium ions compared to that of phosphate species, non-equilibrium complexes with a calcium deficiency can emerge in the system for a short time interval.[12]

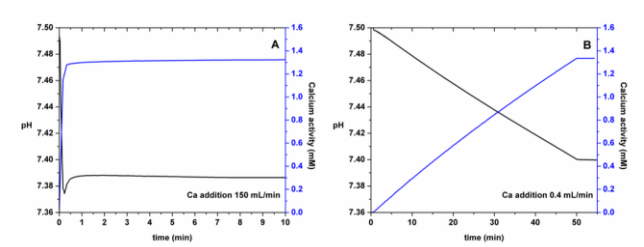

Figure 2. pH (black line) and calcium activity (blue line) profiles of additive-free phosphate solutions with the addition of calcium solution at (A) 150 and (B) 0.4 mL min^{-1} during the s1 of precipitation and titration experiments, respectively. The dashed lines mark the time points at which the calcium addition was complete at each rate.

After equilibration, the pH and Ca signals were stable during s1 and there was no indication of a phase separation in the system. In order to investigate the characteristics of the prenucleation stage, replicate titration experiments were conducted at a low rate of Ca^{2+} addition (0.4 mL min^{-1}) and the potentiometric measurements were compared to the precipitation experiments. Equilibration of pH and calcium activity at same levels under both conditions suggested that the solution speciation at equilibrium was not affected by the rate of Ca^{2+} addition (Figure 2).[11, 12] The pH profile of the titration experiments showed a gradual drop during the calcium addition due to the formation of ion pairs followed by an immediately stable signal (Figure 2B) in contrast to the fluctuations observed in precipitation experiments before the establishment of equilibrium (Figure

2A). The differences in pH profiles were attributed to the augmented formation of unstable complexes or solids (resulting in a larger drop in pH) due to poor mixing during fast addition of calcium, whereas at a sufficiently slow rate the calcium addition did not evoke such instabilities.[12]

Once it was confirmed that the equilibrated solution speciation at s1 was independent of Ca^{2+} addition rate, further analyses were conducted with the titration experiments to investigate the solution speciation at s1 and physical characteristics of the prenucleation species. Slow titration of calcium into the phosphate solution showed a linear relation between the total added and free calcium concentrations (Figure 3), which implied the formation of single Ca^{2+} -based ion complexes in solution (see supplementary information, section D).[36, 37] In addition, measured values of calcium activity showed an excellent fit ($R^2 = 0.999$) with the Minteq model data that only assumes the presence of classical ion pairs such as $[CaHPO_4]^0$ and $[CaH_2PO_4]^+$ (see supplementary information Figure S3). These results are in contrast with some previous studies that postulated the formation of multi-ion association complexes in solution.[11, 12] However, it should be noted that the energy landscape of the initially formed species depends strongly on the starting driving force, which is specific to each experimental procedure.[38]

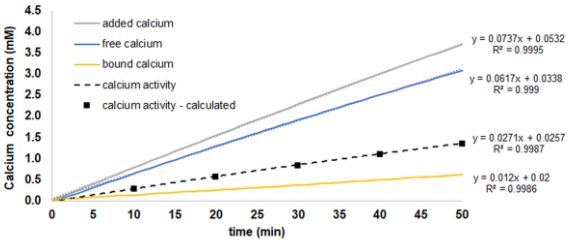

Figure 3. Experimentally measured calcium activity (dashed line) and concentration (straight lines) as a function of time during calcium addition in the titration experiments. Minteq model data

for calcium activity (black squares) at 10 min intervals is overlaid on the experimentally measured values. Ca^{2+} addition rate = 0.4 mL min^{-1}.

In order to inspect the presence of nanometer sized entities in solution, DLS measurements were conducted during titration experiments (Figure 4). Data showed rather stable hydrodynamic radii and low count rates in the prenucleation stage, followed by a sharp increase in both parameters at the proximity of the first discernable drop in pH, remarking the nucleation event. The correlation diagrams also pointed out low correlation coefficients associated with low signal to noise ratio prior to the nucleation event. Thus, based on the titration experiments, we propose single Ca^{2+} - based ion pairs are the main solution species and regard large clusters of multi-complex structures as insignificant components of the equilibrated solution speciation at the prenucleation stage, s1.

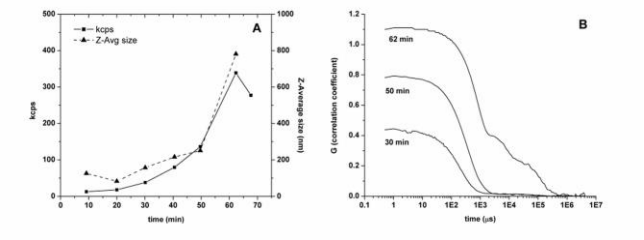

Figure 4. DLS results showing (A) evolution of the derived count rate and hydrodynamic radii (Z-average size) as a function of time during the titration experiment (calcium titration was completed at 50 min and induction time for the given data was recorded as ~60 min) and (B) the correlation diagrams for subsequent time points. The associated correlation data showed increasing correlation coefficient (G) with time, which indicates higher signal to noise ratio. The intercept at G > 1.00 at 62 min indicates sedimentation, which also appeared as an additional descent on the curve that denotes presence of multiple size populations of particles, and as a drop in the count rate.

Following s1, an abrupt drop in both pH and Ca^{2+} activity was detected, followed by a plateau region. FTIR analysis of the first post-nucleation species collected at s2 revealed broad PO_4^{3-} bands around 1020 cm^{-1}, weak band at 875 cm^{-1} associated with HPO_4^{2-} (Figure 5A) and water associated bands and peaks around 3300, 1630 and 640 cm^{-1}. μ-Raman spectroscopy showed a broad band around 950-955 cm^{-1} (Figure 5B). No XRD peaks were detected, which together with the μ-Raman and FTIR results, indicate an amorphous nature (Figure 5C). TEM analysis of precipitates collected during s2 confirmed that during the plateau, only amorphous spherical particles were present (Figure 6A and B). Near the end of the plateau, the presence of a crystalline phase was also detected along with the previously observed amorphous phase (Figure 6C). Thus, it was concluded that the first discernable drop in pH was associated with the precipitation of ACP and the second drop was due to the appearance of a crystalline phase. Electron diffraction of the initial crystals revealed (111) and (210) planes of HA with corresponding d-spacings of 0.389 and 0.309 nm, respectively. Characterization of precipitates at s3 also showed the crystal formation with corresponding peaks in the XRD spectrum (Figure 5C) and sharpening of FTIR and Raman bands. Under these experimental conditions, both OCP and HA are probable phases to nucleate, which can be difficult to differentiate due to their close chemical and structural similarity.[39, 40] However, the absence of a characteristic (100) OCP plane in both electron and X-ray diffraction data throughout and following s3 indicates that OCP lattice was not fully formed during the reaction. It must be noted that these observations do not unequivocally rule out the possible formation of OCP-like layers in terms of structure and composition, but clearly demonstrate that the crystallization pathway did not include OCP as a transient phase.[41]

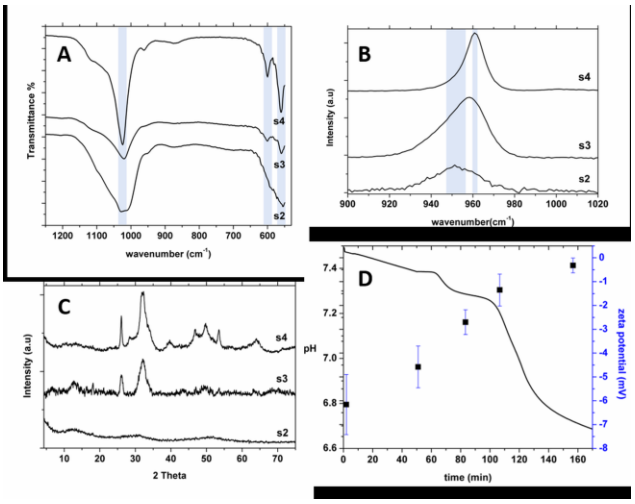

Figure 5. Physicochemical characterization of the intermediate and final products of the precipitation reaction collected at s2 to s4 in the additive-free medium. (A) FTIR, (B) μ-Raman and (C) XRD spectra show the chemical evolution of the precipitates from ACP to HA. The shaded areas in FTIR and μ-Raman spectra highlight the changes in the peak widths and positions. (D) Zeta potential of the particles measured as a function of time and pH during a titration experiment.

Following the nucleation of the crystalline phase, both pH and Ca^{2+} concentration showed a substantial decrease during s3, where ACP was completely transformed to the more stable crystalline phase. TEM analysis showed the co-existence of both amorphous and crystalline phases at the beginning of s3 (Figure 6C). By the time s4 was reached, only HA was present and the prominent (002) and (112/211) planes were evident in both the X-ray and electron diffraction data (Figure 5C and 6D respectively). Note the weak SAED pattern consisting of a mixture of spots and rings and broad peaks of the XRD data, both indicating low crystallinity and/or small crystallite size. Previous studies have reported intermediate phases such as a denser ACP phase, brushite and OCP during transformation of ACP to HA, as well as direct transformation to HA depending on the reaction conditions such as temperature, pH, reactant concentrations and presence of additives.[42] Under the specified experimental conditions, no intermediate crystalline

phase was detected prior to HA formation. During s4, a very slow decrease in both pH and Ca^{2+} signals continued for up to 48 h (data not shown) which indicated further HA growth and maturation (Figure 6E). In the pH range of the corresponding experiments, HPO_4^{2-} dominates the phosphate speciation in solution. Accordingly, an ACP phase reflecting this speciation would be expected to form, which would then be replaced by a nonstoichiometric, hydrogen phosphate rich apatite phase.[41] FTIR analysis of the precipitates collected at s4 showed sharp distinguishable peaks of PO_4^{3-} at 1025 and 962 cm^{-1}; and splitting of the v_4 bending of PO_4^{3-} at 600 and 560 cm^{-1} indicating HA crystallization (Figure 5A).[24] The weak band at 875 cm^{-1} corresponding to HPO_4^{2-} was still present and can be evaluated as an indication of the nonstoichiometric composition (see supplementary information Figure S4). The zeta potential measurements showed how the effective charge on the particles changed with the phase evolution and the accompanying change in the solution pH, where the point of zero charge was approached during HA formation and at a pH value around 6.7 (Figure 5D).

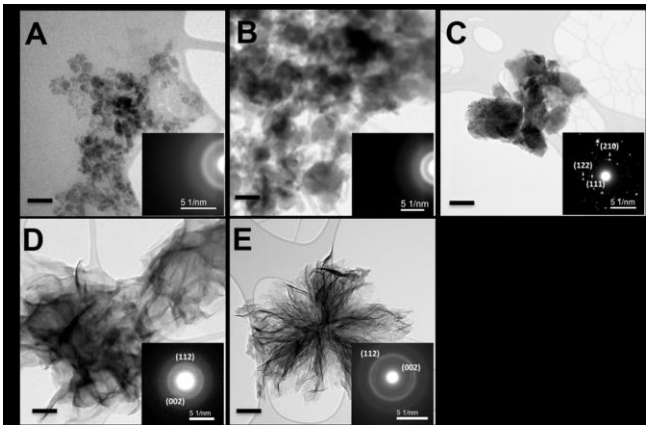

Figure 6. TEM micrographs and corresponding electron diffraction patterns of samples collected during the reaction in the absence of additives; (A) 16-22 min (s2), (B) 33-38 min (s2), (C) 55-60 min (s3), (D) 85-90 min (s3) and (E) after 48 h of aging in the mother liquor (s4). Scale bar denotes: A-B: 50 nm, C-E: 200 nm.

The effects of alginate additives on CaP crystallization

The CaP precipitation experiments were repeated in the presence of alginate derived additives and the same characterization techniques as previously described in section 3.1 were applied to determine their effects on the formation, crystallization and transformation of CaP species. The pH profiles obtained in the presence of additives were similar in shape to each other and to the additive free experiments, albeit across an extended timeframe which was dependent on the type of additive. All featured the same characteristic regions, defined previously as s1-s4, showing an initial stable region, followed by an abrupt drop until a plateau and a second substantial drop before a final stable pH was reached (Figure 7). XRD (see supplementary information Figure S5) and TEM characterization of the intermediate products at s2 showed amorphous precipitates after the first nucleation point for all experiments (Figure 8). Accordingly, the second drop in pH indicated the appearance of the crystalline phase and determined the onset of stage 3. Characterization of the final products by FTIR, Raman and XRD revealed a mixture of OCP and HA when alginate and G-block oligomers were added in the reaction medium, whereas no OCP was detected with M-block additives (see supplementary information Figure S6).

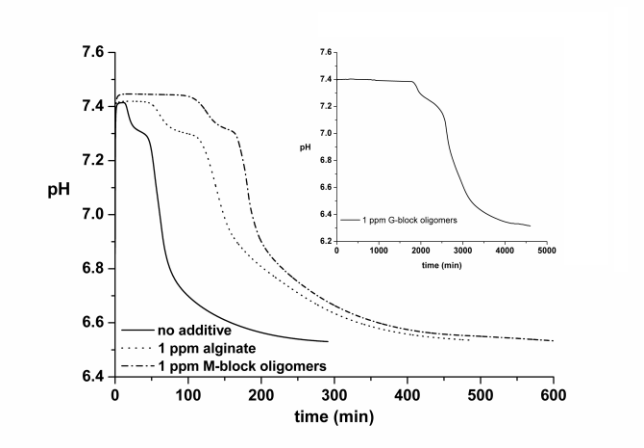

Figure 7. pH profiles of spontaneous precipitation experiments in the absence and presence of the indicated alginate based additives. Inset shows the pH profile of the reaction in the presence of G-block oligomers. Note the substantially different time scales.

As mentioned previously, although the characteristic regions of the pH curves and the initial formation of amorphous phase remained the same in the presence of additives, the duration of each stage was affected (Figure 7). The induction time for ACP precipitation (s1) was prolonged in the presence of additives where short oligomer chains, particularly G-block oligomers, were found to be more effective inhibitors. It should be noted that the thermodynamic calculations were repeated in the presence of additives assuming all G-blocks present in solution bind to calcium ions. The low molar concentration of G-blocks at any experimental condition with respect to the total Ca^{2+} concentration did not cause any significant decrease in the calcium activity (see supplementary information section F). The measured calcium activity at s1 also did not show any significant differences with varying additives (see supplementary information Figure S7). In addition, the measurements of solution viscosity in the presence of additives confirmed that the retardation in reaction progression was not due to an increase in the solution viscosity with the introduction of additives, which can significantly alter reaction kinetics (see supplementary information section G

and Figure S8). Previous studies showed that the presence of additives can alter the ACP solubility and thus affect its induction time as a result of the changing supersaturation with respect to ACP.[19, 43] However pH and calcium activity measurements showed similar values at s2 for all experiments prior to observation of any crystalline particles, which indicates negligible effects of our alginate based additives on ACP solubility. In light of the gathered information, kinetic factors were considered to explain the delayed formation of ACP.

In the presence of oligomers, TEM images of samples collected prior to any abrupt drop in pH (s1) showed small entities initially, with larger structures appearing at later time points (Figure 8). DLS measurements conducted during the titration experiments in the presence of M-block additives showed a steady increase in the count rate and hydrodynamic radii until the nucleation point for ACP was reached and the same characteristics were also reflected on the correlation diagram (Figure 9). However, the calcium activity showed a steady linear increase in good correlation with Minteq calculations and a stable value until the first nucleation point (see supplementary information Figure S9). Thus, the entities observed during s1 were attributed to oligomer assemblies that formed via association with ions/ ion pairs in solution. The ACP precipitates imaged after the nucleation point showed structural similarities to these earlier point assemblies, which suggests a templating effect of the additives. Thus, the prolongation of s1 in the presence of additives were attributed to the interference of the additives with the kinetic variables of classical nucleation (i.e. collision frequency) or stabilization of the intermediates within the template structures. Evidence of kinetic variables controlling the reaction is further supported by the gentle linear growth in radii (~ 6 nm min^{-1}) of the precipitates following the completion of the titration up to ca. 800 nm, compared to an abrupt growth (~ 40 nm min^{-1}) observed under additive free conditions (c.f. Figures 4A & 9A, see supplementary information section C).

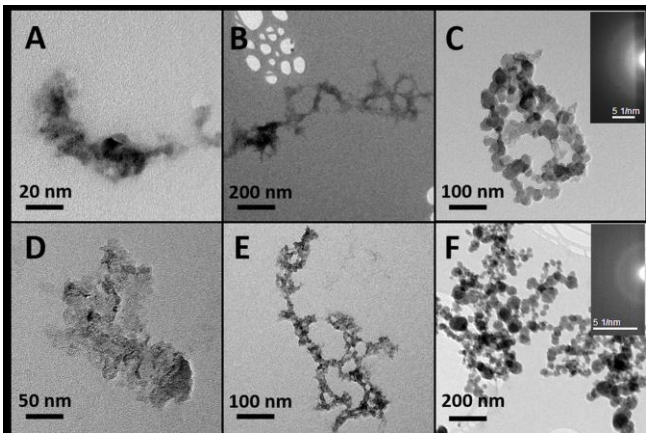

Figure 8. TEM micrographs of samples precipitated in the presence of (A to C) M-block and (D to F) G-block oligomers. Images were collected during s1 (A-B and D-E) and s2 (C and F). SAED patterns showed diffused rings, characteristic for amorphous materials, for all samples (data shown for C and F only).

The presence of polymeric additives can evoke metastable, dense liquid-like precursors via the PILP mechanism.[14, 15] As recently shown in a calcium carbonate system, amorphous clusters can be stabilized in the presence of charged polymers, whereas they were not detected in the absence of additives or individually in the early stages of the reaction, which implied they were not stable before assembly.[17] The pKa values of M- and G-repeating units are 3.38 and 3.65, respectively, and the pKa value of alginate polymer differs only slightly from its monomers, thus, all additives are negatively charged in solution. The molar concentrations of polymer/oligomer chains in the reaction media vary dramatically due to the difference in their molecular weights. Consequently, oligomers introduce significantly higher molar concentration of polymeric molecules in the reaction media. Therefore, for our system we propose a similar mechanism in which electrostatic interactions are the dominant contributors in controlling reaction kinetics. This is highly plausible since the temporal order of ACP formation followed alginate, M-block oligomers and then G-block oligomers and this is also the order of increasing electrostatic strength.

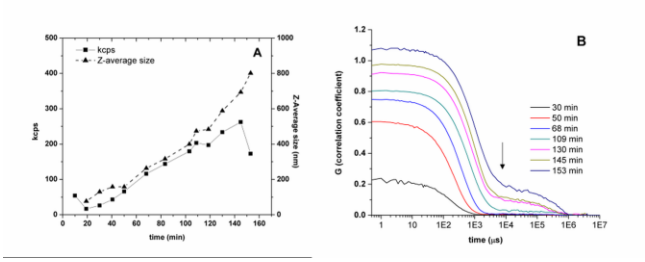

Figure 9. DLS results showing (A) evolution of the derived count rate and Z-average size as a function of time for the precipitation of CaP in the presence of 1 ppm M-block oligomers (calcium titration was completed at 50 min and induction time for the given data was recorded as ~150 min) and (B) the correlation diagrams for subsequent time points. The associated correlation data showed increasing correlation coefficient with time, which indicates higher signal to noise ratio and second descents from 109 min associated with the presence of larger-sized particle populations (shown by the arrow).

s2 was also prolonged when the additives were present in the reaction medium. The beginning of this stage is dominated by ACP formation with the accompanying drop in the pH until the plateau prior to the appearance of any crystalline nuclei. In the presence of alginate and M-block additives, the duration of s2 until reaching the plateau was almost doubled with respect to the additive free experiments, whereas it was most prolonged in the presence of G-block oligomers lasting approximately an order of magnitude longer compared to additive free conditions. These data clearly show the reduced rate of ACP precipitation in the presence of all additives tested. The plateau region of s2 was maintained until the appearance of crystals, which was defined as the second nucleation point. In order to determine this second nucleation point, there should be sufficient crystal nucleation and growth to generate a distinctive change in pH. Previous studies of ACP-mediated crystal formation suggested that the additives can delay crystal nucleation by interfering with heterogeneous nucleation processes on the ACP surface, or by stabilizing this

metastable phase via direct adsorption on the surface.[25, 44] Accordingly, zeta potential measurements of ACP phases precipitated in the presence of additives showed higher negative values compared to additive free controls which therefore verified a surface adsorption mechanism (-10.4 ± 2.5 mV with alginate and -14.8 ± 1.5 mV with M-block oligomers at pH 7.30). Adsorption of additives on the ACP surface is governed by the specific and nonspecific electrostatic interactions between the mineral and the functional groups of the alginate repeating units.[45] Thus, the specific affinity and significantly higher molar concentration of polymeric molecules introduced to the reaction media well explains the prolonged lifetime of ACP most efficiently with G-block oligomers. Carboxyl groups of M-blocks do not have a specific affinity towards calcium ions; however, nonspecific interactions with the ACP surface are still likely to occur via ionic interactions or H-bonding.[30] The difference between alginate and G-blocks is twofold. Alginate polymer contains higher amounts of M-units that do not bind Ca-ions and CaP surfaces as well, as shown by much weaker effect seen for M-block samples. Due to higher molecular weight, the alginate samples also contain lower molar concentration of polymer chains allowing it to occupy a lower number of active sites at the same weight per volume concentration. Yet, the extent of stabilization of ACP in the presence of alginate was comparable to M-block oligomers. This observation indicates that along with the electrostatic and specific interactions caused by the structural and stereochemical compatibility between the alginate repeating units and mineral surfaces, the steric hinderance provided by the high molecular weight alginate can also affect the surface coverage.[46] These results coincide with the recent work of Tao *et al.* that demonstrated the strong correlation between protein adsorption and the prolonged induction times for ACP to HA transformation by high-resolution, in situ atomic force microscopy.[47]

The explicit correlation observed between the lifetime of ACP and adsorption capacity of additives infers a transformation mechanism involving the ACP surface acting as a substrate for heterogeneous crystal nucleation and/or a dissolution-reprecipitation pathway.[40] Under similar experimental conditions, some previous studies have also proposed a solid-state transformation mechanism whereby crystalline domains were reported to form within the ACP particles.[12, 26] The *ex-situ* TEM images collected in this work cannot be used to state the starting point for crystal nucleation with confidence since they are not representative of the entire system in its dynamic state. However, the strong dependence of the emergence of crystalline phase to the surface characteristics of ACP provides convincing support for a solvent-mediated transformation mechanism.

HA proceeds to grow and ACP completely transforms to HA during s3 in the presence of M-block additives. Previous work conducted by our group showed that HA growth was the rate-limiting step of the transformation reaction of brushite to HA under similar experimental conditions.[32] Since ACP is a highly metastable phase with a higher solubility than brushite at constant temperature, it was concluded that s3 was controlled by HA growth where the presence of M-block additives extended the time span by growth inhibition (see supplementary information section H).[21] In the presence of alginate and G-block oligomers, XRD of precipitates collected at s4 showed the distinctive OCP peak at $2\theta = 4.7°$ along with a clear HA spectra (see supplementary information Figure S6). TEM also showed the coexistence of both crystalline phases where small HA crystals were observed together with large OCP plates (Figure 10). Although the crystalline phases were formed at comparable supersaturation levels in all systems, the alginate additives induced a change in the final reaction product. Considering the specific affinity of G-blocks to calcium ions and consequently ACP surfaces, the increasing content of G-blocks can be

responsible for reducing the rate of HA nucleation and allow the formation of kinetically more favorable phases. In addition, growth rate studies revealed that G-block oligomers were highly effective in blocking the active growth sites on HA crystal surfaces (see supplementary information section H). Therefore, OCP mineralization could become kinetically favored in the system as a result of effective suppression of HA formation. In their recent study, Wang *et al.* presented similar results where OCP emerged as an intermediate phase during transformation of ACP to HA, when factors of kinetic origins such as presence of a polymeric additive and/or confinement extended the lifetimes of metastable phases.[48] Emergence of OCP as a result of effective stabilization of metastable phases as shown in these studies can be evaluated as supportive information for the widely discussed role of OCP as an intermediate between ACP and HA during bone formation *in vivo,* where the kinetic control mechanisms on mineral formation are far more efficient.[48, 49]

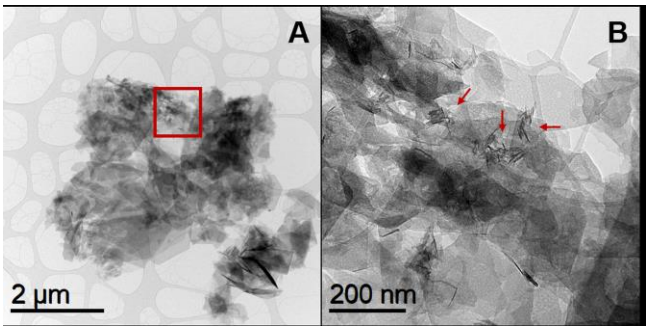

Figure 10. TEM micrographs of final products precipitated in the presence of 1 ppm G-block oligomers showing the large plates of OCP together with small HA crystals pointed by the arrows. The marked area in (A) is shown in higher magnification in (B).

CONCLUSION

We investigated HA formation via an ACP precursor phase by combining potentiometric measurements of pH and calcium activity in solution with comprehensive physicochemical characterization of resulting precipitates as a function of time. The two subsequent stages of ACP and HA formation were determined from the abrupt drops in pH and calcium measurements and the characterization of precipitates showed that each step was associated with the emergence of a separate phase. In additive-free experiments, titration data and thermodynamic calculations demonstrated that the solution speciation was dominated by classical ion pairs present in the prenucleation stage, prior to ACP phase separation in the system which in turn was followed by transformation to HA. In the presence of alginate-based additives, it was shown that compositional variations of the additive molecules determined how they influenced the reaction. ACP nucleation was retarded in all cases due to kinetic hinderance and possible stabilization of PILP-like intermediates. ACP lifetime was also prolonged in all cases due to surface stabilization by the additives and a solvent-mediated transformation mechanism to crystalline phases was proposed. When additives containing G-units were introduced in the system, final precipitates composed of a mixture of OCP and HA via effective suppression of HA formation. We anticipate the findings in this study will improve the understanding of mineralization mechanisms and the roles of additives, and in turn contribute to the design of improved composite biomaterials.

ASSOCIATED CONTENT

Supporting Information. Experimental methods, supporting figures, tables, discussion and references. Supporting figures include additional solution speciation data, characterization spectra

and calcium activity measurements. Additional discussion on titration experiments and solid characterization is presented. Seeded constant composition experiments of HA growth is presented. This material is available free of charge via the Internet at http://pubs.acs.org.

AUTHOR INFORMATION

Corresponding Author

*E-mail: jens-petter.andreassen@ntnu.no

*E-mail: seniz.ucar@ntnu.no

Author Contributions

The manuscript was written through contributions of all authors. All authors have given approval to the final version of the manuscript.

Notes

The authors declare no competing financial interest.

ACKNOWLEDGMENT

The authors would like to thank Ragnhild Sæterli for her assistance with the TEM analyses. This work was supported by the Research Council of Norway (FRINATEK Project 214607). The Research Council of Norway is acknowledged for the support to the Norwegian Center for Transmission Electron Microscopy, NORTEM (197405/F50) and the Norwegian Micro- and Nano-Fabrication Facility, NorFab.

ABBREVIATIONS

HA, hydroxyapatite; ACP, amorphous calcium phosphate; OCP, octacalcium phosphate; CaP, calcium phosphate; PILP, polymer induced liquid precursor; M-, mannuronic acid; G-, guluronic

acid; S, supersaturation; DLS, dynamic light scattering; TEM, transmission electron microscopy; XRD, X-ray diffraction; FTIR, Fourier transform infrared.

REFERENCES

1. Oyen, M. L., The Materials Science of Bone: Lessons from Nature for Biomimetic Materials Synthesis. *MRS Bull.* **2008,** *33*, 49-55.
2. Wang, Y.; Azaïs, T.; Robin, M.; Vallée, A.; Catania, C.; Legriel, P.; Pehau-Arnaudet, G.; Babonneau, F.; Giraud-Guille, M.-M.; Nassif, N., The predominant role of collagen in the nucleation, growth, structure and orientation of bone apatite. *Nat. Mater.* **2012,** *11*, 724-733.
3. Bassett, D. C.; Grover, L. M.; Müller, F. A.; McKee, M. D.; Barralet, J. E., Serum Protein Controlled Nanoparticle Synthesis. *Adv. Funct. Mater.* **2011,** *21*, 2968-2977.
4. Aizenberg, J.; Muller, D. A.; Grazul, J. L.; Hamann, D. R., Direct Fabrication of Large Micropatterned Single Crystals. *Science* **2003,** *299*, 1205-1208.
5. Olszta, M. J.; Cheng, X.; Jee, S. S.; Kumar, R.; Kim, Y.-Y.; Kaufman, M. J.; Douglas, E. P.; Gower, L. B., Bone structure and formation: A new perspective. *Mater. Sci. Eng. R:* **2007,** *58*, 77-116.
6. Weiner, S.; Mahamid, J.; Politi, Y.; Ma, Y.; Addadi, L., Overview of the amorphous precursor phase strategy in biomineralization. *Front. Mater. Sci. China* **2009,** *3*, 104.
7. Combes, C.; Rey, C., Amorphous calcium phosphates: Synthesis, properties and uses in biomaterials. *Acta Biomater.* **2010,** *6*, 3362-3378.
8. Gelli, R.; Ridi, F.; Baglioni, P., The importance of being amorphous: calcium and magnesium phosphates in the human body. *Adv. Colloid Interface Sci.* **2019,** *269*, 219-235.
9. Kashchiev, D.; van Rosmalen, G. M., Review: Nucleation in solutions revisited. *Cryst. Res. Technol.* **2003,** *38*, 555-574.
10. Dey, A.; Bomans, P. H. H.; Müller, F. A.; Will, J.; Frederik, P. M.; de With, G.; Sommerdijk, N. A. J. M., The role of prenucleation clusters in surface-induced calcium phosphate crystallization. *Nat Mater* **2010,** *9*, 1010-1014.
11. Habraken, W. J. E. M.; Tao, J.; Brylka, L. J.; Friedrich, H.; Bertinetti, L.; Schenk, A. S.; Verch, A.; Dmitrovic, V.; Bomans, P. H. H.; Frederik, P. M.; Laven, J.; van der Schoot, P.; Aichmayer, B.; de With, G.; DeYoreo, J. J.; Sommerdijk, N. A. J. M., Ion-association complexes unite classical and non-classical theories for the biomimetic nucleation of calcium phosphate. *Nat. Comm.* **2013,** *4*, 1507.
12. Xie, B.; Halter, T. J.; Borah, B. M.; Nancollas, G. H., Tracking Amorphous Precursor Formation and Transformation during Induction Stages of Nucleation. *Cryst. Growth Des.* **2014,** *14*, 1659-1665.
13. Tao, J.; Fijneman, A.; Wan, J.; Prajapati, S.; Mukherjee, K.; Fernandez-Martinez, A.; Moradian-Oldak, J.; De Yoreo, J. J., Control of Calcium Phosphate Nucleation and Transformation through Interactions of Enamelin and Amelogenin Exhibits the "Goldilocks Effect". *Cryst. Growth Des.* **2018,** *18*, 7391-7400.
14. Gower, L. B.; Odom, D. J., Deposition of calcium carbonate films by a polymer-induced liquid-precursor (PILP) process. *J. Cryst. Growth* **2000,** *210*, 719-734.

15. Ibsen, C. J. S.; Gebauer, D.; Birkedal, H., Osteopontin Stabilizes Metastable States Prior to Nucleation during Apatite Formation. *Chem. Mater.* **2016,** *28*, 8550-8555.
16. Jee, S. S.; Culver, L.; Li, Y.; Douglas, E. P.; Gower, L. B., Biomimetic mineralization of collagen via an enzyme-aided PILP process. *J. Cryst. Growth* **2010,** *312*, 1249-1256.
17. Xu, Y.; Tijssen, K. C. H.; Bomans, P. H. H.; Akiva, A.; Friedrich, H.; Kentgens, A. P. M.; Sommerdijk, N. A. J. M., Microscopic structure of the polymer-induced liquid precursor for calcium carbonate. *Nat. Comm.* **2018,** *9*, 2582.
18. Li, Y.; Chen, X.; Fok, A.; Rodriguez-Cabello, J. C.; Aparicio, C., Biomimetic Mineralization of Recombinamer-Based Hydrogels toward Controlled Morphologies and High Mineral Density. *ACS Appl. Mater. Interfaces* **2015,** *7*, 25784-25792.
19. Boskey, A. L.; Posner, A. S., Conversion of amorphous calcium phosphate to microcrystalline hydroxyapatite. A pH-dependent, solution-mediated, solid-solid conversion. *J. Phys. Chem.* **1973,** *77*, 2313-2317.
20. Mullin, J. W., *Crystallization*. Butterworth-Heinemann: 1997.
21. Cardew, P. T.; Davey, R. J., The Kinetics of Solvent-Mediated Phase Transformations. *Proc. R. Soc. A* **1985,** *398*, 415-428.
22. Jiang, S.; Chen, Y.; Pan, H.; Zhang, Y.-J.; Tang, R., Faster nucleation at lower pH: amorphous phase mediated nucleation kinetics. *Phys. Chem. Chem. Phys.* **2013,** *15*, 12530-12533.
23. Ding, H.; Pan, H.; Xu, X.; Tang, R., Toward a Detailed Understanding of Magnesium Ions on Hydroxyapatite Crystallization Inhibition. *Cryst. Growth Des.* **2014,** *14*, 763-769.
24. Chen, Y.; Gu, W.; Pan, H.; Jiang, S.; Tang, R., Stabilizing amorphous calcium phosphate phase by citrate adsorption. *CrystEngComm* **2014,** *16*, 1864-1867.
25. Jiang, S.; Pan, H.; Chen, Y.; Xu, X.; Tang, R., Amorphous calcium phosphate phase-mediated crystal nucleation kinetics and pathway. *Faraday Discuss.* **2015,** *179*, 451-461.
26. Wang, C.-G.; Liao, J.-W.; Gou, B.-D.; Huang, J.; Tang, R.-K.; Tao, J.-H.; Zhang, T.-L.; Wang, K., Crystallization at Multiple Sites inside Particles of Amorphous Calcium Phosphate. *Cryst. Growth Des.* **2009,** *9*, 2620-2626.
27. Yu, M.; Wang, L.; Zhang, W.; Ganss, B., An Evolutionarily Conserved Subdomain in Amelotin Promotes Amorphous Calcium Phosphate-to-Hydroxyapatite Phase Transition. *Cryst. Growth Des.* **2019,** *19*, 2104-2113.
28. He, W.; Kjellin, P.; Currie, F.; Handa, P.; Knee, C. S.; Bielecki, J.; Wallenberg, L. R.; Andersson, M., Formation of Bone-like Nanocrystalline Apatite Using Self-Assembled Liquid Crystals. *Chem. Mater.* **2012,** *24*, 892-902.
29. Bjornoy, S. H.; Bassett, D. C.; Ucar, S.; Andreassen, J. P.; Sikorski, P., Controlled mineralisation and recrystallisation of brushite within alginate hydrogels. *Biomed. Mater.* **2016,** *11*, 1748-6041.
30. Mørch, Ý. A.; Donati, I.; Strand, B. L., Effect of Ca2+, Ba2+, and Sr2+ on Alginate Microbeads. *Biomacromolecules* **2006,** *7*, 1471-1480.
31. Bjørnøy, S. H.; Bassett, D. C.; Ucar, S.; Strand, B. L.; Andreassen, J.-P.; Sikorski, P., A correlative spatiotemporal microscale study of calcium phosphate formation and transformation within an alginate hydrogel matrix. *Acta Biomater.* **2016,** *44*, 254-266.
32. Ucar, S.; Bjørnøy, S. H.; Bassett, D. C.; Strand, B. L.; Sikorski, P.; Andreassen, J. P., Transformation of brushite to hydroxyapatite and effects of alginate additives. *J. Cryst. Growth* **2016**, 468, 774-780.
33. Haug, A.; Larsen, B.; Smidsrod, O., A Study of Constitution of Alginic Acid By Partial Acid Hydrolysis. *Acta Chem. Scan.* **1966,** *20*, 183-190.

34. Skjakbraek, G.; Larsen, B., Biosynthesis of Alginate - Purification and Characterization of Mannuronan C-5-Epimerase from Azotobacter-Vinelandii. *Carbohydr. Res.* **1985,** *139*, 273-283.
35. Yun, J.; Holmes, B.; Fok, A.; Wang, Y., A Kinetic Model for Hydroxyapatite Precipitation in Mineralizing Solutions. *Cryst. Growth Des.* **2018,** *18*, 2717-2725.
36. Smeets, P. J. M.; Finney, A. R.; Habraken, W. J. E. M.; Nudelman, F.; Friedrich, H.; Laven, J.; De Yoreo, J. J.; Rodger, P. M.; Sommerdijk, N. A. J. M., A classical view on nonclassical nucleation. *Proc. Natl. Acad. Sci. U. S. A.* **2017,** *114*, E7882-E7890.
37. Henzler, K.; Fetisov, E. O.; Galib, M.; Baer, M. D.; Legg, B. A.; Borca, C.; Xto, J. M.; Pin, S.; Fulton, J. L.; Schenter, G. K.; Govind, N.; Siepmann, J. I.; Mundy, C. J.; Huthwelker, T.; De Yoreo, J. J., Supersaturated calcium carbonate solutions are classical. *Sci. Adv.* **2018,** *4* (1).
38. De Yoreo, J. J.; Sommerdijk, N. A. J. M.; Dove, P. M., Nucleation Pathways in Electrolyte Solutions. In *New Perspectives on Mineral Nucleation and Growth: From Solution Precursors to Solid Materials*, Van Driessche, A. E. S.; Kellermeier, M.; Benning, L. G.; Gebauer, D., Eds. Springer International Publishing: Cham, 2017; 1-24.
39. Bigi, A.; Ripamonti, A.; Cojazzi, G.; Gazzano, M.; Roveri, N., Thermal conversion of octacalcium phosphate into hydroxyapatite. *J. Inorg. Biochem.* **1990,** *40,* 293-299.
40. Lotsari, A.; Rajasekharan, A. K.; Halvarsson, M.; Andersson, M., Transformation of amorphous calcium phosphate to bone-like apatite. *Nat. Comm.* **2018,** *9*, 4170.
41. Ibsen, C. J. S.; Chernyshov, D.; Birkedal, H., Apatite Formation from Amorphous Calcium Phosphate and Mixed Amorphous Calcium Phosphate/Amorphous Calcium Carbonate. *Chem. - Eur. J.* **2016,** *22*, 12347-12357.
42. Bar-Yosef Ofir, P.; Govrin-Lippman, R.; Garti, N.; Füredi-Milhofer, H., The Influence of Polyelectrolytes on the Formation and Phase Transformation of Amorphous Calcium Phosphate. *Cryst. Growth Des.* **2004,** *4*, 177-183.
43. Boskey, A. L.; Posner, A. S., Magnesium stabilization of amorphous calcium phosphate: A kinetic study. *Mater. Res. Bull.* **1974,** *9*, 907-916.
44. Chatzipanagis, K.; Iafisco, M.; Roncal-Herrero, T.; Bilton, M.; Tampieri, A.; Kroger, R.; Delgado-Lopez, J. M., Crystallization of citrate-stabilized amorphous calcium phosphate to nanocrystalline apatite: a surface-mediated transformation. *CrystEngComm* **2016,** *18*, 3170-3173.
45. Comeau, P.; Willett, T., Impact of Side Chain Polarity on Non-Stoichiometric Nano-Hydroxyapatite Surface Functionalization with Amino Acids. *Sci. Rep.* **2018,** *8*, 12700.
46. Sikirić, M. D.; Füredi-Milhofer, H., The influence of surface active molecules on the crystallization of biominerals in solution. *Adv. Colloid Interface Sci.* **2006,** *128-130*, 135-158.
47. Tao, J.; Shin, Y.; Jayasinha, R.; Buchko, G. W.; Burton, S. D.; Dohnalkova, A. C.; Wang, Z.; Shaw, W. J.; Tarasevich, B. J., The energetic basis for hydroxyapatite mineralization by amelogenin variants provides insights into the origin of amelogenesis imperfecta. *PNAS* **2019**, 201815654.
48. Wang, Y.-W.; Christenson, H. K.; Meldrum, F. C., Confinement Increases the Lifetimes of Hydroxyapatite Precursors. *Chem. Mater.* **2014,** *26*, 5830-5838.
49. Weiner, S., Transient precursor strategy in mineral formation of bone. *Bone* **2006,** *39*, 431-433.

FOR TABLE OF CONTENTS USE ONLY

Formation of Hydroxyapatite via Transformation of Amorphous Calcium Phosphate in The Presence of Alginate Additives

Seniz Ucar*, a Sindre H. Bjørnøy,b David C. Bassett,b,c Berit L. Strand,d Pawel Sikorski,b and Jens-Petter Andreassen*, a.

a Department of Chemical Engineering, b Department of Physics and d Department of Biotechnology, Norwegian University of Science and Technology, Trondheim, Norway. c Department of Chemical Engineering, University of Birmingham, Birmingham, UK.

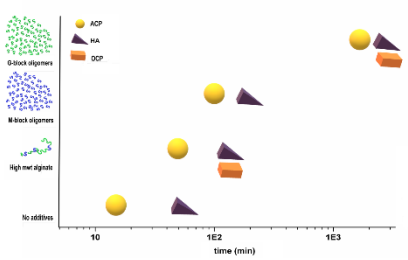

SYNOPSIS. The mineralization pathway of amorphous phase mediated hydroxyapatite formation is influenced strongly by the presence of alginate derived additives in relation to their compositional variations.